CHEMISTRY
A EUROPEAN JOURNAL

DOI: 10.1002/chem.200701037

Supramolecular Solids as a Medium for Single-Crystal-to-Single-Crystal *E*/*Z* Photoisomerization: Kinetic Study of the Photoreactions of Two Zn-Coordinated Tiglic Acid Molecules

Shao-Liang Zheng,*[a] Christophe M. L. Vande Velde,[a, b] Marc Messerschmidt,[a] Anatoliy Volkov,[a] Milan Gembicky,[a] and Philip Coppens*[a]

Abstract: $[Zn(TA)_2(H_2O)_2]$ (H-TA = tiglic acid) has been embedded in a framework composed of CECR (CECR = *C*-ethylcalix[4]resorcinarene) molecules to examine its $E \rightarrow Z$ photoisomerization in a periodic framework. The photoisomerization of tiglic acid in CECR-$[Zn(TA)_2(H_2O)_2]\cdot 4H_2O$ proceeds without the [2+2]-dimerization reaction that often occurs in crystals of uncomplexed analogues, and without breakdown of the crystal lattice that frequently occurs in neat crystals. The two Zn-coordinated TA molecules are located in different size cavities. The rate constants of the isomerization reaction are strongly affected by the size of the reaction cavity. Analysis of the temperature dependence of the reaction rates and the occupancies in the final photostationary state shows that the activation energies and the standard enthalpies of activation are dependent on the difference between the reaction cavities. This is the first quantitative diffraction study of solid-state *E*/*Z* isomerization of a metal-coordinated ligand in a periodic host environment.

Keywords: host–guest systems · inclusion compounds · photoisomerization · reaction cavity

Introduction

The concept of "reaction cavity", originally developed by Cohen to describe photodimerization reaction in crystals,[1] has been applied to explain a number of reactions,[2,3] such as intramolecular hydrogen abstractions,[4] *E*/*Z* photoisomerizations,[5] and other molecular solid-state reactions.[6] While topotactic, single-crystal-to-single-crystal (SCSC) reactions[7,8] offer an opportunity to document the structure of the reactant and its environment to a level of detail that is not possible in any other reaction medium,[2,9] such reactions are rare in the neat crystals. Nevertheless, a number of [2+2][10] and [4+4][11] photodimerizations and intramolecular cyclizations,[12–14] in which molecular migration is minimal have been reported recently.

The multicomponent supramolecular solid state is providing access to an almost unlimited range of novel phases in which photo-reactive molecules can be embedded in a framework of photo-inert building blocks.[15–20] Photoreactions in the framework matrix generally proceed without breakdown of the crystal lattice, so that the progress of the reaction can be monitored by diffraction methods.

E/*Z* photoisomerizations have attracted special interest, as important physiological reactions are triggered by *cis*–*trans* and *trans*–*cis* isomerizations in molecules. Examples are the photoreactions of rhodopsin[21] and photoactive yellow protein (PYP).[22,23] In the case of PYP, the reactive *p*-coumaric chromophore is embedded in a protein envelope, with the surrounding solvent molecules providing a buffer region that can absorb conformational changes of the protein triggered by the isomerization, leading to preservation of the crystal structure. But due to the limited extent of protein scattering, details of the reaction can not be observed at atomic resolution. On the other hand, in neat crys-

[a] Dr. S.-L. Zheng, Dr. C. M. L. Vande Velde, Dr. M. Messerschmidt, Dr. A. Volkov, Dr. M. Gembicky, Prof. Dr. P. Coppens
Department of Chemistry
State University of New York at Buffalo
Buffalo, New York, 14260-3000 (USA)
Fax: (+1) 716 645 6948
E-mail: chem9994@buffalo.edu
coppens@buffalo.edu

[b] Dr. C. M. L. Vande Velde
On leave from the University of Antwerp
Department of Chemistry, Universiteitsplein 1
2610 Wilrijk, Belgium

Supporting information for this article is available on the WWW under http://www.chemeurj.org/ or from the author.

tals the geometry changes on *E*/*Z* isomerization can cause breakdown of the crystal lattice as the reaction proceeds,[24] even though the external shape of the crystals may be perfectly retained.[25] This is often not the case for supramolecular solids.[18,19,26,27] In addition, isolation of a molecule in a supramolecular complex prevents the [2+2] dimerization or polymerization which frequently occur when C=C bonds are stacked in a parallel (or anti-parallel) fashion in crystals.[28]

In preceding work we reported the SCSC *E*/*Z* isomerization of the *E* modification of (*E*)-2-methylbut-2-enoic acid, tiglic acid (HTA, see below) and chloroacrylic acid embedded in a CECR framework (CECR = *C*-ethylcalix[4]resorcinarene),[18,19] the latter reaction starting from both the pure

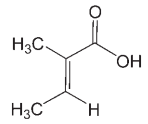

HTA

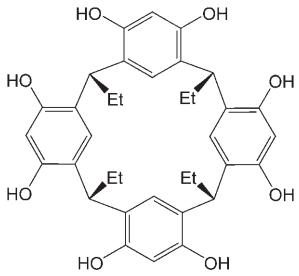

CECR

Z and the pure *E* isomers. Here, we present the first example of the SCSC *E*→*Z* isomerization of a molecule ligated to a group IIB metal atom within a supramolecular framework, CECR-$[Zn(TA)_2(H_2O)_2]\cdot 4H_2O$. The temperature dependence of the kinetic process and the barriers for isomerization on the excited state surface are derived by analysis of the reaction kinetics at different temperatures.

Results and Discussion

Synthetic strategy: Although resorcinarenes, such as CECR, are versatile building blocks which can generate a remarkable variety of different frameworks with bipyridyl-type spacers,[29] only a few examples of *two*-component complexes incorporating large guest molecules are known.[30] HTA is reported to ligate to Zn^{II} to give polymeric chains in which the Zn is four-coordinate.[31] We find that hydrothermal synthesis with a 1:2 benzene/water mixture of $Zn(OH)_2$ and CECR gives a two-component supramolecular host–guest solid, in which distinct $[Zn(TA)_2(H_2O)_2]$ molecules are incorporated in a CECR framework.

Crystal structure at 90 K: The structure of CECR-$[Zn(TA)_2(H_2O)_2]\cdot 4H_2O$ is shown in Figure 1a. The Zn^{II} atom is formally five-coordinate (Table 1) as one of the TA ligands is bidentate and the second monodentate with Zn(1)···O(11) equal to 2.433(4) Å, which is well beyond the values reported for Zn coordinated carboxylic acids.[32] CECR molecules are connected by intermolecular hydrogen bonds [O···O 2.726(3)–2.819(4) Å, Table 2] to form sheets parallel to the *b* axis, which combine with symmetry-related parallel sheets into bilayers parallel to the (110) plane (Figure 1b).

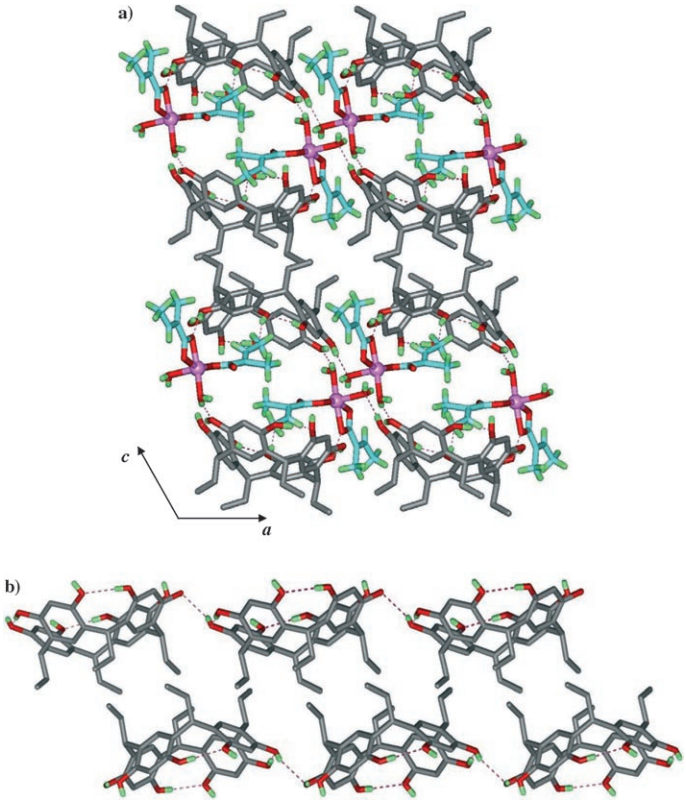

Figure 1. a) 3D-supramolecular architecture viewed along the *b*-axis direction (Zn atom is displayed as a sphere). b) Structure of the bilayers. As shown in a) the Zn^{II} complexes are mainly located in the space between the bilayers.

The space between adjacent bilayers has an effective width of 3.8 Å and consists of double-bowl-shaped cavities with a 7.6×4.3 Å effective cross section.[33] A smaller cavity with 3.6×4.8 Å effective cross section is found between two adjacent CECR molecules within one layer. The two TA ligands in the Zn complex are located within these different cavities, which means that one of the TA ligands is more restricted than the other one. The total free space accounts for 73.7% of the crystal volume. The $[Zn(TA)_2(H_2O)_2]$ molecules are hydrogen-bonded to the hydroxyl oxygen atoms of adjacent CECR molecules [O···O 2.663(3) Å]. Four water molecules are included in each bowl-shaped cavity and linked by hydrogen bonds to oxygen atoms of adjacent CECR's and to the carboxylic oxygen atoms of adjacent TA ligands [O···O 2.602(3)–2.798(3) Å].

The molecular environment of Zn complex is shown in Figure 2. For the TA ligand in the smaller cavity (TA@S),

Table 1. Zn–O bond lengths [Å] in the $[Zn(TA)_2(H_2O)_2]$ complex at 90 K before and after exposure. Atoms in the photoinduced *Z* isomer are labeled with B.

Before exposure			
Zn(1)–O(9)	2.198(3)	Zn(1)–O(12)	2.007(3)
Zn(1)–O(10)	2.097(3)	Zn(1)–O(1W)	2.021(2)
Zn(1)···O(11)	2.433(4)	Zn(1)–O(2W)	2.083(2)
After 2 h exposure			
Zn(1)–O(9)	2.176(5)	Zn(1)–O(12)	2.03(3)
Zn(1)–O(10)	2.06(4)	Zn(1)–O(1W)	2.030(8)
Zn(1)···O(11)	2.426(6)	Zn(1)–O(2W)	2.10(1)
Zn(1B)···O(9B)	2.68(3)	Zn(1B)-O(12B)	1.94(5)
Zn(1B)–O(10B)	2.20(2)	Zn(1B)–O(1WB)	2.02(5)
Zn(1B)···O(11B)	3.14(2)	Zn(1B)–O(2WB)	2.03(7)

Table 2. Hydrogen bond lengths in the CECR-$[Zn(TA)_2(H_2O)_2]\cdot 4H_2O$ complex at 90 K.

D-H···A	*d*(D···A)	∢DHA	D-H···A	*d*(D···A)	∢DHA
O(1)-H(1O)···O(5a)	2.819(4)	153.4	O(5)-H(5O)···O(4)	2.781(4)	170.0
O(2)-H(2O)···O(10b)	2.663(3)	174.2	O(6)-H(6O)···O(7)	2.751(3)	170.9
O(3)-H(3O)···O(2)	2.724(3)	175.2	O(7)-H(7O)···O(2Wc)	2.746(3)	165.7
O(4)-H(4O)···O(4W)	2.703(4)	148.3	O(8)-H(8O)···O(1)	2.726(3)	174.8

[a] $x+1,y,z$. [b] $-x+1,-y+1,-z+1$. [c] $-x+1,-y+2,-z+1$.

analysis of the packing reveals many contacts within the sum of the van der Waals radii on both sides of the (C42=C43–C44) plane, the shortest being 3.470 Å. On the other hand, for the TA ligand in the larger cavity (TA@L), the shortest contacts for the corresponding atoms are > 3.8 Å and occur only on one side of the plane through the corresponding atoms.

***E*→*Z* photoisomerizations**: In the first series of experiments the diffractometer-mounted crystal was exposed to 325 nm light from a 48 mW He/Cd laser at 90 K. This is in the long-wavelength tail of the absorption band, which maximizes homogeneous illumination throughout the crystal.[2] Subsequent measurements were performed at higher temperatures to allow analysis of the temperature dependence of the reaction and derivation of relevant thermodynamic quantities for the solid-state reaction. After a two-hour exposure, the photodifference maps, shown in Figure 3 for TA@S, clearly show light-induced peaks corresponding to a conversion of part of the TA molecules to the *Z* configuration, and depletion of density at the original positions of the TA ligand atoms. In addition the Zn^{II} atom shows a considerable shift, quantified by the subsequent least-squares refinement as 0.22(1) Å. The distance between Zn^{II} and the O(9) oxygen atom increases from 2.176(5) to 2.68(3) Å, which effectively reduces the Zn coordination from five- to four-fold (Table 2), both ligands now being monodentate (Figure 4, Table 1). The dihedral angles between the planes through the four ligand carbon atoms (C41-C42-C43-C44 in TA@S, and C46-C47-C48-C49 in TA@L) before and after the reaction are 6.2(1) and 86.6(3)° in TA@S and TA@L respectively. The larger conformational change in TA@L is attributed to the much larger volume of the reaction cavity. Least squares refinement of the data after exposure indicates that 14.8(5)% of TA@S and 36.6(6)% of TA@L have converted to the *Z* isomer (Table 3), again indicating a pronounced influence of the cavity dimensions on the resulting photostationary state.

At all temperatures, changes in the unit cell volume are less than 0.1% (Table S1, Supporting Information), but in particular for TA@S, the cavity volume per TA increases during the irradiation (Table 4). This increase occurs at the expense of the volume occupied by the solvent molecules.

Analysis of the reaction cavities: As listed in Table 4, the volume increase of the smaller reaction cavity from 92.6 to 117.7 $Å^3$, compared with the smaller increase for the larger cavity, is indicative of the constraints that can be imposed on solid-state reactions by the surrounding matrix. In order to get insight in the effect of the "reaction cavity", an analysis of the interaction[6] between the

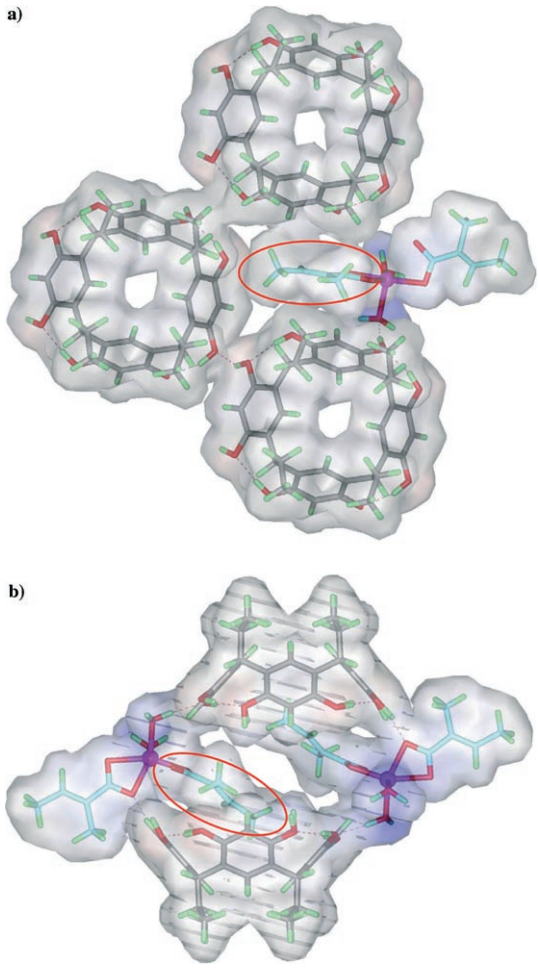

Figure 2. Interactions between $[Zn(TA)_2(H_2O)_2]$ and its host surroundings: a) TA@S. b) TA@L (Zn atom is displayed as a sphere). Surfaces shown are defined by the atomic van der Waals radii.

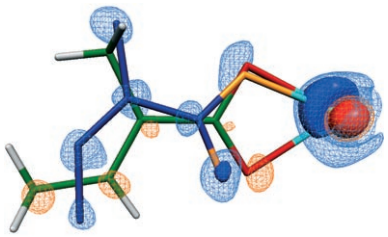

Figure 3. Difference map of the TA@S complexed to Zn^{II} after 2 h exposure (blue: 2.0, light blue: 1.0, orange: −1.0, red: −2.0 e Å^{-3}).

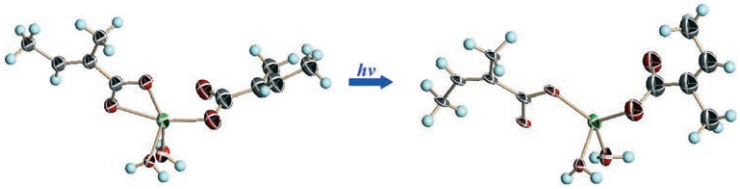

Figure 4. Perspective views showing 50% probability displacement ellipsoids of the Zn^{II} complex before exposure and after 2 h exposure.

Table 3. Conversion ratio for TA ligands at different temperatures and different stages of exposure.

State		90 K/0 h	90 K/1 h	90 K/2 h	90 K/5 h	90 K/8 h
conver ratio [%]	TA@S	0	12.5(6)	14.8(5)	16.2(10)	17.5(10)
	TA@L	0	25.4(7)	34.6(6)	46.0(8)	46.7(8)
State		115 K/ 0 h	115 K/ 1 h	115 K/ 2 h	115 K/ 4 h	115 K/ 8 h
conver ratio [%]	TA@S	0	17.6(9)	19.4(10)	19.9(10)	20.1(11)
	TA@L	0	32.3(7)	42.8(8)	45.9(8)	46.1(8)
State		140 K/ 0 h	140 K/ 0.5 h	140 K/ 1 h	140 K/ 2 h	140 K/ 5 h
conver ratio [%]	TA@S	0	19.2(9)	20.2(9)	22.1(7)	23.4(7)
	TA@L	0	30.9(7)	35.1(5)	45.0(8)	45.3(8)
State		190 K/ 0 h	190 K/ 0.5 h	190 K/ 1 h	190 K/ 2 h	190 K/ 6 h
conver ratio [%]	TA@S	0	19.9(12)	20.1(9)	21.0(10)	21.1(10)
	TA@L	0	34.6(9)	39.6(7)	41.4(7)	43.1(8)

Table 4. Cavity volume of TA ligands and interaction energy (from DFT calculation) between the TA ligand and the surrounding molecules for the *E* and the *Z* isomers.

	TA@L			TA@S		
	E	*Z*	Δ	*E*	*Z*	Δ
TA volume of cavity [Å^3]	153.8	157	3.2	92.6	111.7	8.1
E_{int} [kJ mol^{-1}]	−117.3	−110.9	6.4	262.9	303.8	40.9

TA ligand and the surrounding molecules (Figure 2) has been performed. Although similar intermolecular hydrogen bonds between the hydroxyl oxygen atoms of CECR molecules (host) and the carboxylic oxygen atoms of adjacent TA ligands (guest) exist, E_{int} of TA@L is attractive; while E_{int} of TA@S is repulsive, both for the *E* and the *Z* isomers. This fact suggests that for TA@S, the repulsive interactions override the attractive intermolecular hydrogen bonds due to the size of cavity. Moreover, on exposure, the ligand/cavity interaction energy E_{int} becomes less negative in both cases, but the destabilization is larger for TA@S. All of these indicate that the larger cavity volume favors the isomerization.

Reaction rate and kinetic analysis at 90 K: The conversion fractions of photo-isomerized TA ligand as a function of irradiation time are presented in Figure 5. The curves represent first-order kinetics[34] and can be fitted with exponential functions. For the 90 K experiments the results are: for TA@S, $y = 0.175–0.175(9)\exp[-t/0.899(12)]$ ($R = 0.996$), and for TA@L, $y = 0.467–0.467(4)\exp[-t/1.256(29)]$ ($R = 0.995$), where *y* is the conversion fraction of TA ligand in the solids derived from the structure analyses at each intermediate point, and *t* is the time in hours. Combining these equations with the equation $y_{final}/(1-y_{final}) = k(E\rightarrow Z)/k(Z\rightarrow E)$[35] gives the following rate constants at 90 K: for TA@S, $k(E\rightarrow Z) = 0.19(2)$ h^{-1} and $k(Z\rightarrow E) = 0.92(2)$ h^{-1}; while for TA@L, $k(E\rightarrow Z) = 0.37(2)$ h^{-1} and $k(Z\rightarrow E) = 0.42(2)$ h^{-1}.

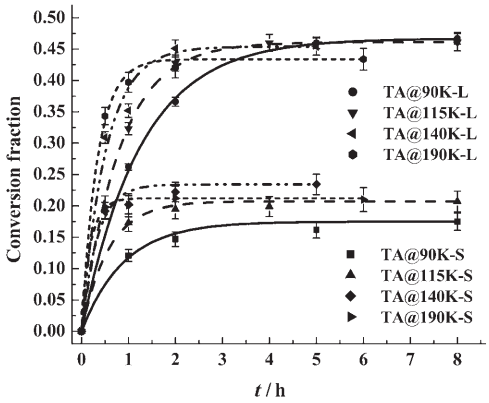

Figure 5. Conversion fractions of Zn-coordinated TA molecules in the small (S, bottom) and large (L, top) cavities as a function of irradiation time at different temperatures (90 K: ——; 115 K: – – –; 140 K: ·· – –; 190 K: -----).

As expected, the reaction is faster in the larger cavity, in which the photostationary state contains almost equal amounts of the two isomers.[36] In the smaller cavity the TA ligand is more restrained and the $Z\rightarrow E$ "back" isomerization is favored over the $E\rightarrow Z$ reaction, as a result an equal distribution is not reached.[18,19]

The external shape of the crystal and its color are not affected by the exposure (Figure S2, Supporting Information), even though the conversion percentage is considerable and both the shape of the guest and its position are affected by the photoisomerization. However, the final *R* factors (Table S1, Supporting Information) increase on exposure, which is attributed to radiation damage rather than to the isomerization.[18]

Analysis of the temperature dependence of the reaction: Comparison of the time dependence of the conversion fractions at 90, 115, 140 and 190 K (Table 5 and Figure 5) shows the reaction rate to increase with temperature, although the stationary state contains slightly less of the product at 190 K, indicating a change in the ratio of the forward and back reactions. The rate increase indicates an activation-energy-limited reaction. The reported rate decrease for SCSC dimerizations above 200 K,[37] due to an increase in the intermolecular distance with temperature, is not expected to occur for this monomolecular reaction.

Table 5. Exponential functions and the rate constant (y: fractional conversion; t [h]).

		$y=A-A\exp(-t/B)$	$k(Z\rightarrow E)$ [h^{-1}]	$k(E\rightarrow Z)$ [h^{-1}]
TA@S	90 K	$y=0.175-0.175(9)\exp[-t/0.899(12)]$ ($R=0.996$)	0.19(2)	0.92(2)
	115 K	$y=0.201-0.201(5)\exp[-t/0.573(49)]$ ($R=0.992$)	0.36(3)	1.38(3)
	140 K	$y=0.234-0.233(14)\exp[-t/0.332(58)]$ ($R=0.990$)	0.70(4)	2.32(4)
	190 K	$y=0.211-0.211(22)\exp[-t/0.202(77)]$ ($R=0.989$)	0.91(4)	4.03(4)
TA@L	90 K	$y=0.467-0.467(4)\exp[-t/1.256(29)]$ ($R=0.995$)	0.37(2)	0.42(2)
	115 K	$y=0.461-0.461(4)\exp[-t/0.810(18)]$ ($R=0.997$)	0.57(2)	0.67(2)
	140 K	$y=0.453-0.453(26)\exp[-t/0.549(26)]$ ($R=0.993$)	0.82(3)	1.00(3)
	190 K	$y=0.431-0.431(11)\exp[-t/0.336(25)]$ ($R=0.995$)	1.29(3)	1.68(3)

A generalized mechanism for singlet and triplet state photoisomerization has been presented by Lewis et al. (Figure 6 and S1, Supporting Information).[38] The qualitative aspects of the diagram are in agreement with conical intersection treatments, which similarly involve an activation energy on the path between the excited state and the transition state from which the return to the initial state or the formation of the product occurs.[39,40] The overall isomerization rate constant k for the forward and back reactions will depend on 1) the extinction coefficient of each of the two isomers; 2) the oscillator strength of the photo-induced excitation to the reactive (π^*) excited state; 3) the rate constant of the process of $S_1\rightarrow{}^1P^*$,[41–43] which is dependent on the height of the barrier on the excited state surface; 4) the relative probabilities (α and $1-\alpha$) that the intermediate state $^1P^*$ decays to the E and Z ground states, $S_0(E)$ and $S_0(Z)$.

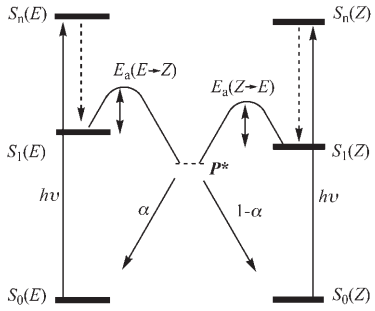

Figure 6. Potential energy diagram for E/Z isomerization.

Absorption spectra of solutions show the absorbance of the E and Z isomers for tiglic acid at 325 nm to be almost identical,[18] whereas TDDFT calculations of E and Z isomers for tiglic acid and their Zn compounds indicate the HOMO–π^* energy gaps and oscillator strengths (Table 6 and Figure S2, Supporting Information) to be practically identical for the E and Z isomers, in agreement with the experimental observation. The ratio of the rate constants will therefore be strongly dependent on the relative activation energies, E_a, and the relative efficiencies of the transition from the transition state back to the initial state or to the product state labeled α and $1-\alpha$ respectively in Figure 6.

Table 6. TDDFT calculated excited state energy separations of E and Z isomers for tiglic acid and their Zn compounds.

Energy separation	HTA		$Zn(TA)_2(H_2O)_2$	
	E E [eV] (f)	Z E [eV] (f)	E E [eV] (f)	Z E [eV] (f)
S_0–S_1	4.880 (0.001)	4.889 (0.001)	4.710 (0.000)	4.570 (0.000)
S_0–S_2	5.905 (0.323)	6.014 (0.359)	4.734 (0.004)	4.601 (0.001)
S_0–S_3	6.982 (0.067)	6.989 (0.081)	5.206 (0.006)	5.282 (0.006)

The Arrhenius plots of the E/Z isomerization rate,[44,45] shown in Figure 7, give the activation energies listed in Table 7. An alternative plot of $\ln(k/T)$ vs $1/RT$, based on the transition state theory of Eyring,[44,46] is shown in Figure 8, with results listed in Table 8. Both plots show the barriers for the $E\rightarrow Z$ and $Z\rightarrow E$ isomerizations to be lower in the small cavity and thus indicate a pronounced effect of the crystal matrix on the solid state reaction.

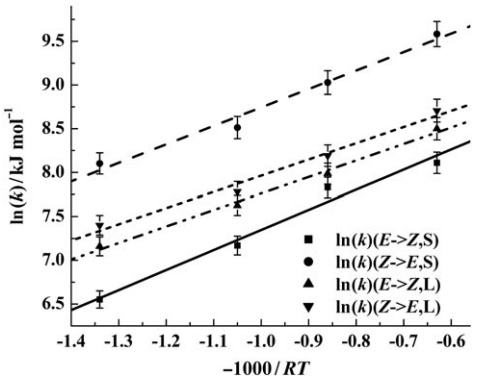

Figure 7. Arrhenius plots of isomerization rates as a function of temperature ($E\rightarrow Z$,S: ——; $Z\rightarrow E$,S: – – –; $E\rightarrow Z$,L: ·· – –; $Z\rightarrow E$,L: -----).

Table 7. Activation energy E_a and pre-exponential factor A for Z/E isomerization of the TA ligand in the small and large cavities derived from the Arrhenius plots.[a]

	$E\rightarrow Z$		$Z\rightarrow E$	
	TA@S	TA@L	TA@S	TA@L
E_a [kJ mol^{-1}]	2.3 (3)	1.8(1)	2.1(2)	1.9(1)
A [10^{-3} s^{-1}]	1.18	1.16	4.05	1.36

[a] Arrhenius expression: $\ln(k)=\ln(A)-E_a/RT$, see Figure 7. Values of A only have a relative meaning, as they depend on the photon flux incident on the crystals and the absorbance.

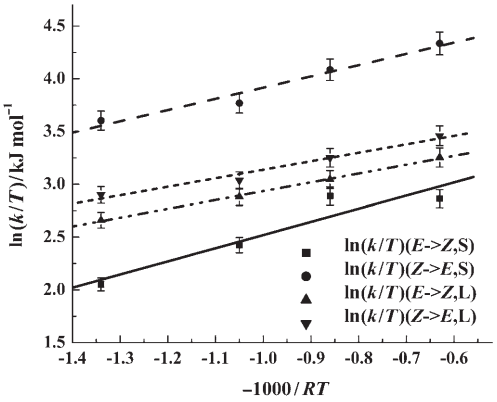

Figure 8. Eyring plot of the isomerization rates as a function of temperature ($E\rightarrow Z$,S: ——; $Z\rightarrow E$,S: -----; $E\rightarrow Z$,L: ·· – –; $Z\rightarrow E$,L: -----).

Table 8. Standard enthalpies of activation$\Delta H^{\neq}$ for Z/E isomerization of the TA ligand in the small and large cavities derived from the Eyring plots ($\ln(k/T)=A-\Delta H^{\neq}/RT$, Figure 8).

	$E\rightarrow Z$		$Z\rightarrow E$	
	TA@S	TA@L	TA@S	TA@L
$\Delta H^{\neq}$ [kJ mol^{-1}]	3.3(3)	2.9(2)	3.1(3)	2.8(2)

Concluding Remarks

We conclude that supramolecular photocrystallography allows quantitative analysis of solid state reactions which in neat crystals are likely to lead to crystal breakdown. The analysis of the SCSC $E\rightarrow Z$ photoisomerization of Zn-coordinated tiglic acid shows a pronounced effect of the crystalline environment on the kinetics of the isomerization. The analysis described here and related studies reported elsewhere[18,19] indicate the potential of supramolecular frameworks to enhance our understanding of photochemical processes in molecular crystals. Martinez has calculated a fs-scale conversion rate for the isolated ethylene molecule.[47] The reaction in the solid state are obviously much slower, and their rate can be tuned by changing the temperature, which implies that the intermediate state may be investigated by time-resolved diffraction methods.[20,48]

The ability to monitor chemical reactions of molecules confined within an inert periodic framework is of particular importance in the developing field of time-resolved diffraction,[20] as it points the way to methods for elucidating the mechanism of chemical reactions with pump-probe techniques.

Experimental Section

Synthesis of CECR–$[Zn(TA)_2(H_2O)_2]\cdot 4H_2O$: Freshly prepared $Zn(OH)_2$ (0.05 mmol), HTA (0.1 mmol) and CECR (0.05 mmol) were mixed with benzene (1 mL) and water (2 mL) in a thick-walled tube. The sealed tube was allowed to stay at 100 °C for 24 h, followed by cooling to room temperature over 30 h. Pale yellow crystals appeared during the cooling period (yield 72 %). Elemental analysis calcd (%) for $C_{46}H_{66}O_{18}Zn$: C 56.82, H 6.84; found: C 57.31, H 6.80.

Photoreaction and X-ray crystallography: Full details of the experimental procedures followed have been reported in a previous publication.[18] To minimize the dependence of the reaction rate on the volume and shape of the crystals used at different temperatures, specimen crystals with dimensions $0.06\times0.10\times0.24$ mm were cut from the same needle crystal ($0.06\times0.10\times1.6$ mm size), and mounted along the longest distance on the diffractometer. Only one crystal was used for successive irradiations at the same temperature.

Data were collected at 90 K on a Bruker APEXII CCD diffractometer installed at a rotating anode source ($Mo_{K\alpha}$ radiation, $\lambda=0.71073$ Å), and equipped with an Oxford Cryosystems nitrogen flow apparatus. 0.3° scans in ω were used with the detector positioned at $2\theta=20°$. Data integration up to 0.82 Å resolution was carried out using SAINT V7.*34* with reflection spot size optimization. Absorption corrections were made with the program SADABS. After the initial data collection the crystal was exposed at 90 K to 325 nm light from a 48 mW He/Cd laser for accumulated periods of 1, 2, 5, 8 h. It was rotated around the ϕ axis during irradiation. One hour after completion of each step of the irradiation, X-ray data were collected at 90 K. The parent structure was solved by direct methods and refined by least-squares methods against F^2 using SHELXS-97 and SHELXL-97. For the parent structure, non-hydrogen atoms were refined anisotropically, the hydroxy H atoms were located in difference maps after which the riding model was applied. Other hydrogen atoms were positioned at idealized positions and refined in the same way. For the structures after irradiation, all non-hydrogen atoms of the product were located in Fourier photodifference maps, calculated with coefficients F_0(exposed)$-F_0$(pre-exposure), and then refined with restraints and constraints of the geometrical and thermal parameters of the reactant and product atoms, as described in the supplementary material of an earlier publication.[18] The riding model was used for the hydrogen atoms. The percentage of the reactant in the crystal was treated as a variable in the refinements. The same procedure was used for data collected at 115, 140 and 190 K.

Crystal data as well as details of data collection and refinement are summarized in Table S1 (Supporting Information), while selected geometrical parameters of the Zn^{II} complex and hydrogen bond parameters at 90 K are listed in Tables 1 and 2 respectively. The Fourier difference maps were produced with the XD-2006 program package,[49] and the molecular drawings with Weblab Viewer Pro. 4.0.[50] Full details: CCDC-625461–625462 and 648902–648919 contain the supplementary crystallographic data for this paper. These data can be obtained free of charge from The Cambridge Crystallographic Data Centre via www.ccdc.cam.ac.uk/data_request/cif.

Theoretical calculations: The BSSE-correlated calculations ($E_{int}=E_{AB}^{(AB)}-E_A^{(AB)}-E_B^{(AB)}$) on the reaction cavity/reactant energies were performed at the B3LYP level at the X-ray geometry with X–H bond lengths extended to standard neutron diffraction distances.[51] The Gaussian03 suite of programs was used with a 6-31++G** basis set for the light atoms and the LanL2DZ set with an effective core potential for Zn.[52] TDDFT calculations of the E and Z isomers for tiglic acid and Zn-coordinated tiglic acid at the same level with the same basis set were also performed. Starting with the X-ray geometries, the structures were optimized by energy minimization.

Acknowledgements

Support of this work by the National Science Foundation (CHE0236317) and the Petroleum Research Fund of the American Chemical Society (PRF32638AC3) is gratefully acknowledged. C.V.V wishes to thank the University of Antwerp for a one-year mandate as a postdoctoral research assistant.

[1] a) M. D. Cohen, G. M. J. Schmidt, F. I. Sonntag, *J. Chem. Soc.* **1964**, 2000–2013; b) M. D. Cohen, *Angew. Chem.* **1975**, *87*, 439–447; *Angew. Chem. Int. Ed. Engl.* **1975**, *14*, 386–394.

[2] A. E. Keating, M. A. Garcia-Garibay, In *Photochemical Solid-to-Solid Reactions in Organic and Inorganic Photochemistry* (Eds.: V. Ramamurthy, K. S. Schanze), Marcel Dekker, **1998**, and references therein.

[3] a) V. Ramamurthy, K. Venkatesan, *Chem. Rev.* **1987**, *87*, 433–481; b) R. G. Weiss, V. Ramamurthy, G. S. Hammo, *Acc. Chem. Res.* **1993**, *26*, 530–536; c) R. S. H. Liu, G. S. Hammo, *Acc. Chem. Res.* **2005**, *38*, 396–403.

[4] Y. Ohashi, T. Hosoya, T. Ohhara, *Crystallogr. Rev.* **2006**, *12*, 83–123.

[5] A. Natarajan, J. T. Mague, K. Venkatesan, T. Arai, V. Ramamurthy, *J. Org. Chem.* **2006**, *71*, 1055–1059.

[6] H. E. Zimmerman, E. E. Nesterov, *Acc. Chem. Res.* **2002**, *35*, 77–85, and references therein.

[7] a) H. W. Kohlshutter, *Z. Anorg. Allg. Chem.* **1918**, *105*, 121; b) G. M. J. Schmidt, *Solid State Photochemistry*, Verlag Chemie, New York, **1976**.

[8] G. Halder, C. Kepert, *Aust. J. Chem.* **2006**, *59*, 597–604.

[9] "Organic Solid State Reactions" in *Topics in Current Chemistry, Vol. 254* (Ed.: F. Toda), Springer, **2005**, and references therein.

[10] I. Turowska-Tyrk, *Acta Crystallogr. Sect. B* **2003**, *59*, 670–675.

[11] a) I. Turowska-Tyrk, E. Trzop, *Acta Crystallogr. Sect. B* **2003**, *59*, 779–786; b) M. Kaftory, V. Shteiman, T. Lavy, J. R. Schffer, J. Yang, V. Enkelmann, *Eur. J. Org. Chem.* **2005**, 847–853.

[12] See for example: a) M. Leibovitch, G. Olovsson, J. R. Scheffer, J. Trotter, *J. Am. Chem. Soc.* **1997**, *119*, 1462–1463; b) M. Leibovitch, G. Olovsson, J. R. Scheffer, J. Trotter, *J. Am. Chem. Soc.* **1998**, *120*, 12755–12769.

[13] I. Turowska-Tyrk, E. Trzop, J. R. Scheffer, S. Chen, *Acta Crystallogr. Sect. B* **2006**, *62*, 128–134.

[14] a) N. Feeder, K. Honda, *Mol. Cryst. Liq. Cryst.* **1998**, *313*, 327–334; b) K. Honda, F. Nakanishi, N. Feeder, *J. Am. Chem. Soc.* **1999**, *121*, 8246–8250.

[15] a) X. Gao, T. FriščiĆ, L. R. MacGillivray, *Angew. Chem.* **2004**, *116*, 234–238; *Angew. Chem. Int. Ed.* **2004**, *43*, 232–236; b) T. FriščiĆ, L. R. MacGillivray, *Z. Kristallogr.* **2005**, *220*, 351–363, and references therein.

[16] a) H. Hosomi, S. Ohba, K. Tanaka, F. Toda, *J. Am. Chem. Soc.* **2000**, *122*, 1818–1819; b) T. Lavy, Y. Sheynin, M. Kaftory, *Eur. J. Org. Chem.* **2004**, 4802–4808, and references therein.

[17] a) K. Tanaka, F. Toda, E. Mochizuki, N. Yasui, Y. Kai, I. Miyahara, K. Hirotsu, *Angew. Chem.* **1999**, *111*, 3733–3736; *Angew. Chem. Int. Ed.* **1999**, *38*, 3523–3526; b) K. Tanaka, F. Toda, E. Mochizuki, N. Yasui, Y. Kai, I. Miyahara, K. Hirotsu, *Tetrahedron* **2000**, *56*, 6853–6865; c) T. Lavy, M. Kaftory, *CrystEngComm* **2007**, *4*, 123–127, and references therein.

[18] S.-L. Zheng, M. Messerschmidt, P. Coppens, *Acta Crystallogr. Sect. B* **2007**, *63*, 644–649.

[19] S.-L. Zheng, M. Messerschmidt, P. Coppens, *Chem. Commun.* **2007**, 2735–2737.

[20] a) P. Coppens, B.-Q. Ma, O. Gerlits, Y. Zhang, P. Kulshrestha, *CrystEngComm* **2002**, *4*, 302–309; b) P. Coppens, S.-L. Zheng, M. Gembicky, M. Messerschmidt, P. M. Dominiak, *CrystEngComm* **2006**, *8*, 735–741.

[21] H. Tsukamoto, A. Terakita, Y. Shichida, *Proc. Natl. Acad. Sci. USA* **2005**, *102*, 6303–6308.

[22] S. Rajagopal, M. Schmidt, S. Anderson, H. Ihee, K. Moffat, *Acta Crystallogr. Sect. D* **2004**, *60*, 860–871.

[23] E. D. Getzoff, K. N. Gutwin, U. K. Genick, *Nat. Struct. Biol.* **2003**, *10*, 663–668.

[24] J. Bregman, K. Osaki, G. M. J. Schmidt, F. I. Sonntag, *J. Chem. Soc.* **1964**, 2021–2030.

[25] K. Tanaka, T. Hiratsuka, S. Ohba, M. R. Naimi-Jamal, G. Kaupp, *J. Phys. Org. Chem.* **2003**, *16*, 905–912.

[26] G. S. Ananchenko, K. A. Udachin, J. A. Ripmeester, T. Perrier, A. W. Coleman, *Chem. Eur. J.* **2006**, *12*, 2441–2447.

[27] R. Arad-Yellin, S. Brunie, B. S. Green, M. Knossow, G. Tsoucaris, *J. Am. Chem. Soc.* **1979**, *101*, 7529–7537.

[28] I. Abdelmoty, V. Buchholz, L. Di, C. Guo, K. Kowitz, V. Enkelmann, G. Wegner, B. M. Foxman, *Cryst. Growth Des.* **2005**, *5*, 2210–2217.

[29] See for example: a) L. R. MacGillivray, K. T. Holman, J. L. Atwood, *J. Supramol. Chem.* **2001**, *1*, 125; b) L. R. MacGillivray, J. L. Reid, J. A. Ripmeester, *Chem. Commun.* **2001**, 1034–1035; c) B.-Q. Ma, Y.-G. Zhang, P. Coppens, *J. Org. Chem.* **2003**, *68*, 9467–9472; d) B.-Q. Ma, P. Coppens, *Cryst. Growth Des.* **2004**, *4*, 1377–1385.

[30] a) S.-L. Zheng, P. Coppens, *Cryst. Growth Des.* **2005**, *5*, 2050–2059; b) S.-L. Zheng, M. Gembicky, M. Messerschmidt, P. Dominiak, P. Coppens, *Inorg. Chem.* **2006**, *45*, 9281–9289.

[31] W. Clegg, J. T. Cressey, D. R. Harbron, B. P. Straughan, *J. Chem. Crystallogr.* **1994**, *24*, 211–217.

[32] F. H. Allen, O. Kennard, D. G. Watson, L. Brammer, A. G. Orpen, R. Taylor, *International Tables for Crystallography, Vol. C* (Ed.: A. J. Wilson), Kluwer, Dordrecht, **1992**, p. 749.

[33] A. L. Spek, *PLATON, A Multipurpose Crystallographic Tool*; Utrecht University, Utrecht (The Netherlands), **2003**.

[34] I. Turowska-Tyrk, *J. Phys. Org. Chem.* **200**4, 17, 837–847.

[35] a) J. De Paula, P. W. Atkins, *Physical Chemistry*, W. H. Freeman, **2001**, 7th ed., pp. 876; b) J. I. Steinfeld, J. S. Francisco, W. L. Hase, *Chemical Kinetics and Dynamics*, Prentice Hall, **1998**, 2nd ed., pp. 23–24.

[36] K. Takagi, T. Shichi, *Photophysics and Photochemistry in Clay Minerals, in Solid State and Surface Photochemistry* (Eds.: V. Ramamurthy, K. S. Schanze), Marcel Dekker, New York, **2003**.

[37] M. Hasegawa, *Chem. Rev.* **1983**, *83*, 507–518.

[38] a) F. D. Lewis, D. M. Bassani, *J. Am. Chem. Soc.* **1993**, *115*, 7523–7524; b) F. D. Lewis, D. M. Bassani, R. A. Caldwell, D. J. Unett, *J. Am. Chem. Soc.* **1994**, *116*, 10477–10485.

[39] G. Groenhof, M. Bouxin-Cademartory, B. Hess, S. P. de Visser, H. J. C. Berendsen, M. Olivucci, A. E. Mark, M. Robb, *J. Am. Chem. Soc.* **2004**, *126*, 4228–4233.

[40] a) M. Garavelli, F. Bernardi, A. Cembran, *Computational Photochemistry* (Ed.: M. Olivucci), Elsevier, Amsterdam, **2005**, pp. 191–223; b) S. Olsen, A. Tommiolo, C. Ko, L. Manohar, K. Lamothe, T. J. Martinez, *Computational Photochemistry* (Ed.: M. Olivucci), Elsevier, Amsterdam, **2005**, pp. 225–401, and references therein.

[41] a) G. Orlandi, P. Palmien, G. Poggi, *J. Chem. Soc. Faraday Trans. 2* **1981**, *77*, 71; b) J. Michl, V. Bonacic-Koutecky, *Electronic Aspects of Organic Photochemistry*, Wiley-Interscience, New York, **1990**, p. 310.

[42] M. Said, J.-P. Malrieu, *Chem. Phys. Lett.* **1983**, *102*, 312.

[43] The energy of the perpendicular intermediate (^{l}P*) is not known, but it is presumably lower than that of the singlet state. See refs. [39], [41] and [42].

[44] J. De Paula, P. W. Atkins, *Physical Chemistry*, W. H. Freeman, 7th ed., **2001**, pp. 807–809.

[45] N. J. Turro, *Modern Molecular Photochemistry* University Science Books, Sausalito, CA, **1991**.

[46] K. J. Laidler, *Chemical Kinetics*, Harper & Row, New York, **1987**.

[47] T. J. Martinez, *Acc. Chem. Res.* **2006**, *39*, 119–126.

[48] P. Coppens, I. I. Vorontsov, T. Graber, M. Gembicky, A. Yu. Kovalevsky, *Acta Crystallogr. Sect. A* **2005**, *61*, 162–172, and references therein.

[49] A. Volkov, P. Macchi, L. J. Farrugia, C. Gatti, P. Mallinson, T. Richter, T. Koritsanszky, XD2006—A Computer Program Package for Multipole Refinement, Topological Analysis of Charge Densities and Evaluation of Intermolecular Energies from Experimental and Theoretical Structure Factors, **2006**.

[50] *Weblab Viewer Pro. 4.0*, Molecular Simulations Inc., San Diego, CA, **1997**.

[51] F. H. Allen, O. Kennard, D. G. Watson, L. Brammer, A. G. Orpen, R. Taylor, In *International Tables for Crystallography, Vol. C* (Ed.: A. J. Wilson), Kluwer Academic Publishers, Dordrecht, **1992**, pp.685–706.

[52] Gaussian03, Revision C.02, M. J. Frisch, G. W. Trucks, H. B. Schlegel, G. E. Scuseria, M. A. Robb, J. R. Cheeseman, V. G. Zakrzewski, J. A. Jr., Montgomery, R. E. Stratmann, J. C. Burant, S. Dapprich, J. M. Millam, A. D. Daniels, K. N. Kudin, M. C. Strain, O. Farkas, J. Tomasi, V. Barone, M. Cossi, R. Cammi, B. Mennucci, C. Pomelli, C. Adamo, S. Clifford, J. Ochterski, G. A. Petersson, P. Y. Ayala, Q. Cui, K. Morokuma, D. K. Malick, A. D. Rabuck, K. Raghavachari, J. B. Foresman, J. Cioslowski, J. V. Ortiz, B. B. Stefanov, G. Liu, A. Liashenko, P. Piskorz, I. Komaromi, R. Gomperts, R. L. D. Martin, J. Fox, T. Keith, M. A. Al-Laham, C. Y. Peng, A. Nanayakkara, C. Gonzalez, M. Challacombe, P. M. W. Gill, B. Johnson, W. Chen, M. W. Wong, J. L. Andres, C. Gonzalez, M. Head-Gordon, E. S. Replogle, J. A. Pople, Gaussian, Inc., Pittsburgh, PA, **2003**.

Received: July 6, 2007
Published online: October 23, 2007

